Title

X-Ray Crystallographic Analysis of NifB with a Full Complement of Clusters: Structural Insights into the Radical SAM-Dependent Carbide Insertion During Nitrogenase Cofactor Assembly

Journal

Angewandte Chemie International Edition, 60(5)

ISSN

1433-7851

Authors

Kang, Wonchull
Rettberg, Lee A
Stiebritz, Martin T
et al.

Publication Date

2021-02-01

DOI

10.1002/anie.202011367

Peer reviewed

Published in final edited form as:

Angew Chem Int Ed Engl. 2021 February 01; 60(5): 2364–2370. doi:10.1002/anie.202011367.

Crystallographic analysis of NifB with a full complement of clusters: Structural insights into the radical SAM-dependent carbide insertion during nitrogenase cofactor assembly

Wonchull Kang[+,a], **Lee A. Rettberg**[+,a], **Martin T. Stiebritz**[a], **Andrew J. Jasniewski**[a], **Kazuki Tanifuji**[a], **Chi Chung Lee**[a], **Markus W. Ribbe**[a,b], **Yilin Hu**[a]

[a]Department of Molecular Biology & Biochemistry, University of California, Irvine, Irvine, CA 92697-3900 (USA)

[b]Department Chemistry, University of California, Irvine, Irvine, CA 92697-2025 (USA)

Abstract

NifB is an essential radical SAM enzyme for the assembly of an 8Fe core of the nitrogenase cofactor. Here we report the crystal structures of *Methanobacterium thermoautotrophicum* NifB without (apo *Mt*NifB) and with (holo *Mt*NifB) a full complement of three [Fe_4S_4] clusters. Both apo and holo *Mt*NifB contain a partial TIM barrel core; yet, unlike apo *Mt*NifB that is structurally disordered outside the TIM barrel, holo *Mt*NifB is fully assembled and competent in cofactor biosynthesis. Of the three [Fe_4S_4] clusters in holo *Mt*NifB, the canonical radical SAM (RS)-cluster, like those in other radical SAM enzymes, is coordinated by three Cys ligands; whereas the adjacently positioned K1- and K2-clusters, representing the precursor to an 8Fe cofactor core, are each coordinated by one His and two Cys ligands. Prediction of substrate channels, combined with *in silico* docking of SAM in holo *Mt*NifB, suggests plausible binding of SAM between the RS- and K2-clusters and putative paths for entry of SAM and exit of products of SAM cleavage, thereby providing important mechanistic insights into the radical SAM-dependent carbide insertion concomitant with cofactor core formation.

Graphical Abstract

yilinh@uci.edu, mribbe@uci.edu.

[+]These authors contributed equally.

Supporting information for this article is given via a link at the end of the document.

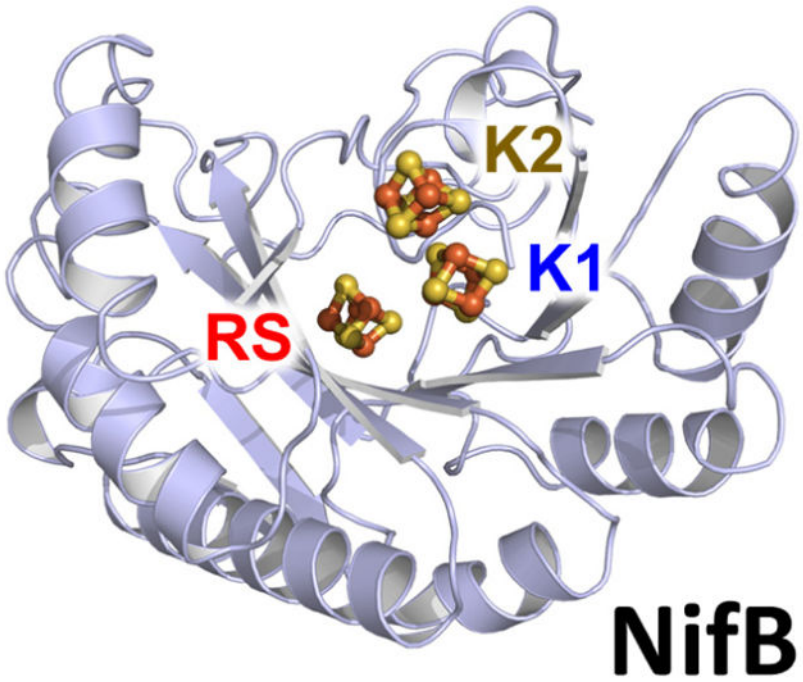

NifB is an essential radical SAM enzyme for the assembly of an 8Fe core of the nitrogenase cofactor. Here we report the crystal structures of *Methanobacterium thermoautotrophicum* NifB without and with a full complement of three [Fe_4S_4] clusters, which provide important mechanistic insights into the radical SAM-dependent carbide insertion concomitant with the formation of a cofactor core.

Keywords

nitrogenase; metalloenzyme; carbide insertion; radical SAM enzyme; cofactor core formation

Introduction

Nitrogenase is a versatile metalloenzyme that catalyzes the ambient reduction of N_2 to NH_3, and CO or CO_2 to hydrocarbons, at its cofactor site.[1–5] Designated the M-cluster, the cofactor of the Mo-nitrogenase has a composition of [(*R*-homocitrate)$MoFe_7S_9C$] and is arguably one of the most complex metallocofactors found in Nature. Biosynthesis of the M-cluster has attracted substantial attention because this cofactor is biologically important and chemically unprecedented. NifB plays a central role in this process, receiving two 4Fe fragments from the ‘upstream’ assembly apparatus NifS/U, transforming them into an 8Fe core of the M-cluster, and passing it on to the ‘downstream’ assembly apparatus NifEN for further maturation into an M-cluster prior to delivery of the M-cluster to its target binding site in NifDK (Figure S1a). A member of the radical *S*-adenosyl-L-methionine (SAM) enzyme family,[6–11] NifB contains a canonical CxxxCxxC motif for the coordination of a SAM-binding [Fe_4S_4] cluster (designated the SAM-cluster; generally termed the RS-cluster in radical SAM enzymes), as well as a number of conserved ligands for the ligation of

a pair of [Fe_4S_4] clusters (designated the K-cluster).[12–14] Upon incubation with SAM, NifB catalyzes the coupling and rearrangement of the two [Fe_4S_4] modules of the K-cluster (designated K1 and K2) into an [Fe_8S_9C] precursor of the M-cluster (designated the L-cluster) concomitant with the insertion of a SAM-derived carbide into the central cavity and a sulfite-derived '9^{th} S' into the belt region of the cluster.[15–18] Formation of the L-cluster, which represents an all-iron structural homolog of the M-cluster, points to a novel biosynthetic route to bridged, high-nuclearity metalloclusters that hinges on the radical SAM-dependent carbide insertion on NifB.

Previous studies of the homologous NifB proteins from *Azotobacter vinelandii* and *Methanosarcina acetivorans* have led us to propose a radical SAM-dependent pathway of carbide insertion concomitant with the K- to L-cluster transformation on NifB.[15–18] This pathway begins with an S_N2-type transfer of a methyl group from one equivalent of SAM to the K2 module of the K-cluster (Figure S1b, ①). Subsequently, a 5′-deoxyadenosyl radical (5′-dA•) is generated via binding and homolytic cleavage of a second equivalent of SAM at the RS-cluster and used to abstract a hydrogen atom from the K2-bound methyl group (Figure S1b, ②). The resultant methylene radical then initiates the coupling and rearrangement of the K1- and K2-modules into an L-cluster while undergoing further deprotonation in a process involving a facile histidine ligand of the K1-module, leading to the formation of an interstitial carbide in the center of the L-cluster (Figure S1b, ③). In support of this proposal, a recently reported crystal structure of NifB from *Methanotrix thermoacetophila* reveals the partial triose phosphate isomerase (TIM) barrel structure that is characteristic of radical SAM enzymes, as well as the presence of an RS-cluster and a K1-module on this NifB protein. However, the K2-module, which hosts two key events of carbide insertion, namely, the initial methyltransfer and the subsequent hydrogen atom abstraction from the methyl group, is notably missing from this structure.[19] While it is unclear whether the absence of K2 from the *M. thermoacetophila* NifB protein is correlated with the absence of the nitrogenase-encoding genes from this organism,[20] the incomplete cluster composition apparently results in substantial structural disorder in certain key regions of this protein. Therefore, it is necessary to perform structural characterization of NifB species from nitrogenase-containing organisms that contain a full complement of clusters in order to probe the mechanism of carbide insertion concomitant with cofactor core formation by this unique radical SAM enzyme.

Results and Discussion

The NifB protein from *Methanobacterium thermoautotrophicum*, a thermophilic methanogen containing nitrogenase-encoding genes in its genome, is a perfect candidate for investigations along this line. Heterologously expressed in *E. coli* and reconstituted with FeS clusters *in vitro*, this NifB protein (designated holo *Mt*NifB) was shown by biochemical and EPR characterizations to have a full complement of RS- and K-clusters and capable of catalyzing the K- to L-cluster transformation upon incubation with SAM.[21] Crystallization of the FeS-reconstituted, holo *Mt*NifB in the presence of dithionite yielded brown crystals that diffracted to a resolution of 3 Å (PDB ID: 7JMB; Table S1). Previously established by biochemical characterizations as a monomer in solutions,[21] the holo *Mt*NifB forms a 'crystallographic dimer' in each asymmetric unit, with the two monomers nearly identical to

each other and showing a Cα deviation of only 0.33 Å (Figure S2a). Spanning from residue 13 to residue 276 (of a total of 288 amino acids), the core structure of holo *Mt*NifB consists of a partial TIM barrel that is characteristic of many radical SAM enzymes (Figure 1a,b; Figure S3) In addition, β-strands S6 and S7 (part of the section connecting β-strands S5 and S8) align with β-strand S2 (part of the section connecting β-strand S1 and α-helix H2) to form a three-stranded antiparallel β-sheet that is situated right next to the partial TIM barrel; and the C- and N-termini of the protein are brought together by a pair of antiparallel β-strands S11 and S1 (Figure 1a,b). Strikingly, there are electron densities in the Fo-Fc omit and anomalous difference Fourier maps of *Mt*NifB that correspond to three [Fe_4S_4] clusters (Figure 2a,b), all of which contained within the space 'walled off' by the partial TIM barrel structure (Figure 1a; Figure S5a). One of them is the canonical RS-cluster, which is held by two loops flanking β-strand S2; whereas the other two represent the adjacently positioned K1- and K2-modules of the K-cluster, with K1 anchored by β-strand S5 along with a loop leading to α-helix H1 and another loop following β-strand S1, and K2 housed in a loop between β-strands S10 and S11 (Figure 1a,b). Interestingly, the K1- and K2-modules are harbored in the flexible regions near the solvent-exposed N- and C-termini, respectively; whereas the RS-cluster is housed in the flexible regions flanking β-strand S2. Such a structural flexibility could facilitate the interactions between the clusters that occur during the dynamic biosynthetic events hosted by NifB.

Structural analysis of the *Mt*NifB protein without FeS reconstitution (designated apo *Mt*NifB) provided further insights into the functionalization of NifB via cluster incorporation. Contrary to holo *Mt*NifB that yielded brown crystals, crystallization of the apo *Mt*NifB resulted in colorless crystals that diffracted to a resolution of 1.7 Å (PDB ID: 7JMA; Table S1). Apo *Mt*NifB has the partial TIM barrel structure mostly preserved in its structure (Figure 1c; Figure S5b) and, compared to the corresponding regions in its holo counterpart, it shows a Cα deviation of only 0.47 Å (Figure S2b). However, the flexible regions carrying part or all ligands of the three clusters, including (*i*) the N-terminus region that carries one Cys ligand for the K1-module, (*ii*) the C-terminus region that carries two Cys ligands for the K2-module, and (*iii*) the loop between β-strand S2 and α-helix H2 that carries one Cys ligand for the RS-cluster, are disordered and absent from the structure of apo *Mt*NifB (Figure 1d; Figure S6). Similarly, the NifB protein from *M. thermoacetophila* (designated *Mtta*NifB), which does not contain the K2-module, also consists of a partial TIM barrel in its core but has the K2-binding region at the C-terminus disordered and absent from the structure (Figure S5c; Figure S6).[19] Together, these observations point to the partial TIM barrel structure as a basic structural framework of NifB; yet, the incorporation of the full complement of clusters is crucial for ordering the remainder of the protein structure, which completes the assembly of holo NifB while functionalizing it as a biosynthetically competent enzyme.

A closer examination of residues surrounding the clusters of holo *Mt*NifB shed important light on their unique coordination patterns. The initial identification of the residues closely interacting with the RS-cluster (Cys^{38}, Cys^{42}, Cys^{45}), the K1-module (Cys^{18}, Cys^{115}, His^{31}) and the K2-module (Cys^{260}, Cys^{263}) was accomplished through refinement of the crystal structure of holo *Mt*NifB (Figure 2a,b); yet, the 3-Å resolution of this structure did not allow modeling of these [Fe_4S_4] clusters other than placing perfect 'cubes' within the

corresponding electron densities. In order to obtain a more realistic representation of the cluster geometries, we performed DFT optimizations on minimal models containing either the RS-cluster or the K1/K2-cluster pair. Upon structural optimization, all clusters show typical cluster geometries with rhombic Fe_2S_2 leaflets (Figure S7). On average, the Fe-S and Fe--Fe distances of DFT-optimized clusters agree well with those derived from the Fe K-edge XAS/EXAFS analysis of holo *Mt*NifB (Figure S8), providing strong validation for the DFT-optimized structures of these clusters and allowing for better assessment of the bonding distances of the cluster ligands.

Based on their DFT-optimized geometries, the canonical RS-cluster has the characteristic 3-Cys ligation pattern, with Cys^{38}, Cys^{42} and Cys^{45} coordinating its three Fe atoms at 2.2, 2.3 and 2.3 Å, respectively; whereas both K1- and K2-modules have a distinct two Cys/one His ligation pattern, with Cys^{18}, Cys^{115} and His^{31} coordinating three Fe atoms of K1 at 2.3, 2.3 and 2.0 Å, respectively, and Cys^{260}, Cys^{263} and His^{24} coordinating three Fe atoms of K2 at 2.3, 2.3 and 2.3 Å, respectively (Figure S7). Such an 'open' coordination pattern of all three clusters is crucial for the functionality of NifB, with the fourth, differentiated Fe atom of the RS-cluster 'free' and ready to bind SAM, and the K1 and K2 each having a 'free' Fe site as well as a 'soft' His ligand that facilitate the initial methyl attachment to K2 and the subsequent coupling of K1 and K2 concomitant with carbide insertion. Of the two His ligands coordinating K1 and K2, the His^{31} ligand of K1 was identified in the corresponding position of two homologous methanogen NifB proteins by ESEEM spectroscopy,[12,14] and its counterpart in *M. acetivorans* NifB was further probed by combined mutagenic and XAS/EXAFS studies.[12] Interestingly, this His ligand was shown to be 'lost' upon coupling of K1 and K2 into an L-cluster, and mutation of this ligand to Ala resulted in an unfinished cluster intermediate with a putative CH_x species bridged between the K1- and K2-derived subcubanes.[12] These observations imply a dual role of this facile His ligand in structurally assisting the proper coupling between K1 and K2 and concurrently facilitating carbide formation via deprotonation of the methyl-derived radical. The His^{24} ligand, on the other hand, was previously 'unseen' by ESEEM in the NifB protein from *M. acetivorans*.[12,13] Occupying a position that is either conserved in place or one position shifted in other methanogen NifB proteins (Figure S9), this His residue could assume a similar role as His^{31} in holding the cluster in proper orientation for coupling while facilitating deprotonation of the methyl-derived radical.

Having assessed the location and coordination of the three clusters in holo *Mt*NifB, we then used the software CAVER to identify potential substrate channels in this protein (Figure 3). Excitingly, the top three candidates of potential substrate channels all merge at the K2-cluster, where two SAM-related events occur: the initial transfer of the SAM-derived methyl group, and the subsequent hydrogen atom abstraction of the methyl group by a SAM-derived 5'-dA• radical (*see* Figure S1b). One of the three channels, which has its entrance formed by β-strand S2 and its flanking loops (Figure 3b, *Channel 1*), runs largely perpendicular to β-strands S2/S5/S8/S9 and routes via the RS-cluster to K2; whereas the other two channels, which have their entrances sharing the loop following β-strand S9 and additionally consist of the loop connecting β-strand S2 and α-helix H2 (Figure 3c, *Channel 2*) and the loop connecting β-strands S10 and S11 (Figure 3c, *Channel 3*), respectively, run largely parallel to β-strands S8/S9 and extend from the protein surface to K2. One plausible scenario in

light of this observation is that *Mt*NifB may use *Channel 1* for the entry and binding of SAM to the RS-cluster. In support of this argument, a SAM molecule can be modeled by the molecular docking software Glide between the RS- and K2-clusters with a good docking score (gscore)/energy of −8.75 kcal/mol (Figure 4a). Interacting with strictly conserved residues Gly^{57}, Gly^{90}, Asn^{194} and Pro^{225}, this SAM molecule is coordinated through its amino nitrogen and carboxylate group to the differentiated Fe site of the RS-cluster, as well as two Fe atoms—one from K1 and the other from K2—through its ribose hydroxyl group (Figure 4a). Notably, the methyl and adenosyl groups of the SAM molecule are positioned in reasonably close distances to K2, suggesting that both methyltransfer and hydrogen atom abstraction might occur through such a binding pattern of SAM despite the fact that methyltransfer follows an S_N2-type mechanism and does not require electron transfer from the reduced RS-cluster. Moreover, the bent conformation of the SAM molecule allows it to align its methionine moiety with *Channel 1* and its adenosyl moiety along *Channels 2* and *3* (Figure 4b,c). Given the spatial limit of the 'catalytic cavity' between the three NifB-associated clusters, it is likely that *Channel 2* or *Channel 3* could be used as exit routs for the (by)products of the reaction (*i.e.*, SAH, methionine and 5'-dAH) to accommodate the entry and binding of the next SAM molecule via *Channel 1*.

Interestingly, the entrance of *Channel 1* is 'closed' in the structure of the K2-deficient *Mtta*NifB protein (Figure S10). The fact that this NifB protein was crystallized in the presence of SAM but was free of SAM in its crystal structure[19] is consistent with the presence of a 'closed' substrate channel that prevents the access of SAM. More importantly, this observation points to the necessity of having both K1- and K2-modules inserted in place—a process accompanied by structural rearrangements of the NifB protein—as the prerequisite for 'opening' the substrate channel and allowing the SAM-related biosynthetic reactions to take place. Such a sequence of events refutes the argument[19] made on the basis of the K2-deficient *Mtta*NifB structure against both K1 and K2 being precursor modules of the 8Fe core of the M-cluster and casts doubt on the suggestion[19] that this incomplete form of NifB represents a mechanistically competent intermediate during the process of cofactor core formation. Indeed, the K2-deficient *Mtta*NifB has its RS-cluster coordinated by a fourth Cys ligand (Cys^{62}) and its K1-cluster interacting with a Glu residue (Glu^{65}) nearby (Figure S11a); whereas in contrast, the corresponding Cys^{51} and Glu^{52} residues in holo *Mt*NifB are located far away from the respective clusters (Figure S11b). The ligation of the RS-cluster by a 'hard' cysteinyl ligand at its 'unique iron' site, the unusual interaction of the K1-module with a Glu residue, and the substantial structural disorder in the key region housing the K2-module collectively point to the structural incompleteness of the K2-deficient *Mtta*NifB. While arguments can be made in support of this K2-depleted NifB species being representative of an intermediate prior to the insertion of K2 and the concomitant functionalization of NifB, the absence of nitrogenase-encoding genes from the genome of its host organism, *M. thermoacetophila*,[20] raises questions as to what function is carried out by this NifB homolog under physiological conditions, whether a K2-module is required for its function, and what type of product is generated if K2 is inserted alongside K1 into this protein.

Conclusion

The existence of NifB homologs in both nitrogenase-containing organisms (*e.g.*, *M. thermoautotrophicus* and *M. acetivorans*)[21] and non nitrogenase-containing organisms (*e.g.*, *M. thermoacetophila*)[20] falls well within the functionally diverse characteristics of the fascinating radical SAM enzyme family (Figure S12; Figure S13). Having a partial TIM barrel as a common structural core, the radical SAM enzymes vary dramatically in their 'accessory' components such as additional domains and auxiliary clusters. The formate-lyase activating enzyme (PFLae), which has no 'accessory' components other than the radical SAM core, is perhaps the simplest member of radical SAM enzyme family that shares a good degree of structural homology with *Mt*NifB except for the absence of the three antiparallel β-strands (Figure S12b).[26] Lipoyl synthase (LipA) and MoaA are two other examples of radical SAM enzymes with strong homology to *Mt*NifB in the core structure (Figure S12c,d)[27,28] and, contrary to PFLae, each of these enzymes has an auxiliary $[Fe_4S_4]$ cluster in addition to the RS-cluster. Similar to the K1- and K2-modules in *Mt*NifB, the auxiliary $[Fe_4S_4]$ clusters in LipA and MoaA are not fully coordinated, each having three Cys ligands and an 'open' Fe site that allows the cluster to either facilitate sulfur donation (LipA) or substrate activation (MoaA) during catalysis. The locations of these auxiliary clusters, however, are at the 'extensions' of the core structure and a lot more distant than K1 or K2 from their respective RS-clusters. Matching holo *Mt*NifB in the number of non RS-clusters are the anaerobic sulfatase maturating enzyme (anSME) and the peptide-modifying enzyme (SuiB) (Figure S13a,b),[29,30] two radical SAM enzymes containing two auxiliary $[Fe_4S_4]$ clusters that function in substrate binding or electron transport. Yet, unlike the K1- and K2-modules in holo *Mt*NifB, the two auxiliary clusters in anSME and SuiB are each coordinated by 4 Cys ligands and situated in distinct domains other than the radical SAM core.

Perhaps the best analog to NifB in term of the mode-of-action is RlmN, a radical SAM enzyme involved in the methylation of ribosomal RNA (Figure S13c).[31] Despite being distinct in their respective functions, the actions of both RlmN and NifB involve methyltransfer from one equivalent of SAM, followed by hydrogen atom abstraction from the methyl group by a 5'-dA• radical derived from a second equivalent of SAM. However, contrary to RlmN that transfers the methyl group to a Cys residue (Cys^{355}) prior to the substrate, NifB transfers the methyl group directly onto a sulfide atom of the K2-cluster via an S_N2-type mechanism. Both reaction pathways then continue with hydrogen atom abstraction from the methyl group, which yields a methylene radical that either initiates the methylation of C2 of adenosine 2503 by RlmN or enables the insertion of carbide by NifB concomitant with the coupling of K1 and K2 into an L-cluster. Interestingly, when the structure of holo *Mt*NifB is superimposed with that of the SAM-treated RlmN, the methylated Cys^{355} residue of RlmN is situated right between the SAM moiety bound in this protein and the K2 module in holo *Mt*NifB (Figure S14). Perhaps even more strikingly, the Cys^{118} residue of RlmN, which is proposed to be involved in the abstraction and 'return' of a proton during the methylation of C2 of adenosine 2503, occupies a position close to the His^{31} residue of *Mt*NifB, which is proposed to be involved in the deprotonation of the initial methylene radical *en route* to the formation of a fully deprotonated carbide ion (Figure S14).

While clearly distinct in their identities and the reactions they catalyze, the Cys^{355}/Cys^{118} pair in RlmN and the K2(sulfide)/His^{31} pair in *Mt*NifB seem to parallel each other in functionality, illustrating a certain common theme in the operation modes of the widely diversified family of radical SAM enzymes. The *Mt*NifB structure reported herein provides an important platform for further investigation into the structural-functional relationship of this enzyme, which is crucial for unravelling the intricate mechanism of radical SAM-dependent carbide insertion during the process of nitrogenase cofactor assembly.

Supplementary Material

Refer to Web version on PubMed Central for supplementary material.

Acknowledgements

This work was supported by NIH-NIGMS grant GM67626 (to M.W.R. and Y.H.). We thank the staff at the Stanford Synchrotron Radiation Lightsource beamline 12-2 and the Advanced Light Source beamline 8.3.1 for technical support in X-ray diffraction data collection. Beamline 8.3.1 at the Advance Light Source is operated by the University of California Office of the President, Multicampus Research Programs and Initiatives grant MR-15–328599, the National Institutes of Health (R01 GM124149 and P30 GM124169), Plexxikon Inc. and the Integrated Diffraction Analysis Technologies program of the US Department of Energy (DOE), Office of Biological and Environmental Research. The Advanced Light Source (Berkeley, CA) is a national user facility operated by Lawrence Berkeley National Laboratory on behalf of the US Department of Energy (DOE) under contract no. DEAC02–05CH11231, Office of Basic Energy Sciences. Stanford Synchrotron Radiation Lightsource, SLAC National Accelerator Laboratory, is supported by the US Department of Energy (DOE), Office of Science, Office of Basic Energy Sciences, under contract no. DE-AC02–76SF00515. The SSRL Structural Molecular Biology Program is supported by the US Department of Energy (DOE), Office of Biological and Environmental Research, and by the NIH National Institutes of General Medical Sciences (NIGMS) (Grant P41GM103393).

References

[1]. Burgess BK, Lowe DJ, Chem. Rev1996, 96, 2983. [PubMed: 11848849]
[2]. Rees DC, et al., Philos. Trans. A Math. Phys. Eng. Sci2005, 363, 971. [PubMed: 15901546]
[3]. Rutledge HL, Tezcan FA, Chem. Rev2020, 120, 5158. [PubMed: 31999100]
[4]. Jasniewski AJ, Lee CC, Ribbe MW, Hu Y, Chem. Rev2020, 120, 5107. [PubMed: 32129988]
[5]. Seefeldt LC, et al., Chem. Rev2020, 120, 5082. [PubMed: 32176472]
[6]. Frey PA, Hegeman AD, Ruzicka FJ, Crit. Rev. Biochem. Mol. Biol2008, 43, 63. [PubMed: 18307109]
[7]. Broderick JB, Duffus BR, Duschene KS, Shepard EM, Chem. Rev2014, 114, 4229. [PubMed: 24476342]
[8]. Vey JL, Drennan CL. Chem. Rev2011, 111, 2487. [PubMed: 21370834]
[9]. Mulliez E, Duarte V, Arragain S, Fontecave M, Atta MM. Front. Chem2017, 5, 17. [PubMed: 28361051]
[10]. Lanz ND, Booker SJ, Biochim. Biophys. Acta2015, 1853, 1316. [PubMed: 25597998]
[11]. Banerjee R, J. Biol. Chem2015, 290, 3962. [PubMed: 25477525]
[12]. Rettberg LA, et al., Nat. Commun2020, 11, 1757. [PubMed: 32273505]
[13]. Rettberg LA, et al., Nat. Commun2018, 9, 2824. [PubMed: 30026506]
[14]. Wilcoxen J, et al., J. Am. Chem. Soc2016, 138, 7468. [PubMed: 27268267]
[15]. Wiig JA, Hu Y, Lee CC, Ribbe MW, Science2012, 337, 1672. [PubMed: 23019652]
[16]. Wiig JA, Hu Y, Ribbe MW, Nat. Commun2015, 6, 8034. [PubMed: 26259825]
[17]. Tanifuji K, et al., Nat. Chem2018, 10, 568. [PubMed: 29662207]
[18]. Jasniewski AJ, et al., Angew. Chem. Int. Ed. Engl2019, 58, 14703. [PubMed: 31411369]
[19]. Fajardo AS, et al., J. Am. Chem. Soc2020, 142, 11006. [PubMed: 32476412]

[20]. The *nifD* and *nifK* genes that encode the subunits of nitrogenase, characterized by the presence of distinct P- and M-cluster ligands, are absent from the genome of *M. thermoacetophila* based on BLAST search performed at https://img.jgi.doe.gov/.

[21]. Fay AW, Wiig JA, Lee CC, Hu Y, Proc. Natl. Acad. Sci. U.S.A2015, 112, 14829. [PubMed: 26627238]

[22]. The PyMOL Molecular Graphics System, Version 2.0Schrödinger, LLC.

[23]. Chovancova E, et al., PLoS Comput. Biol2012, 8, e1002708. [PubMed: 23093919]

[24]. Friesner RA, et al., J. Med. Chem2004, 47, 1739. [PubMed: 15027865]

[25]. Maestro, Schrödinger, LLC, New York, NY, 2020

[26]. Vey JL, et al., Proc. Natl. Acad. Sci. U.S.A2008, 105, 16137. [PubMed: 18852451]

[27]. McLaughlin MI, et al., Proc. Natl. Acad. Sci. U.S.A2016, 113, 9446. [PubMed: 27506792]

[28]. Hänzelmann P, Schindelin H, Proc. Natl. Acad. Sci. U.S.A2004, 101, 12870. [PubMed: 15317939]

[29]. Davis KM, et al., Proc. Natl. Acad. Sci. U.S.A2017, 114, 10420. [PubMed: 28893989]

[30]. Goldman PJ, et al., Proc. Natl. Acad. Sci. U.S.A2013, 110, 8519. [PubMed: 23650368]

[31]. K Boal A, et al., Science2011, 332, 1089. [PubMed: 21527678]

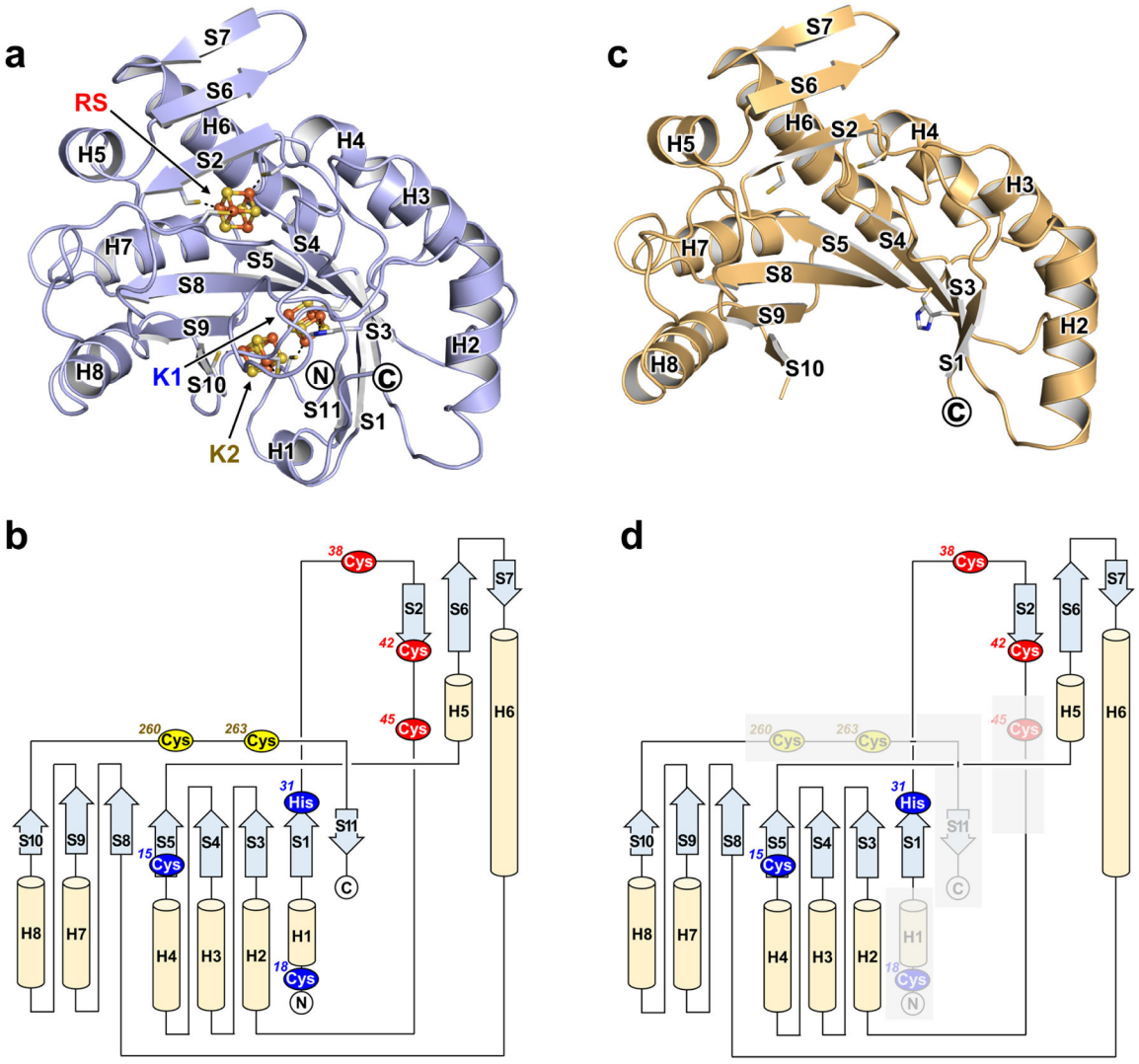

Figure 1.

Crystal structures of holo and apo *Mt*NifB. Ribbon presentations of the structures of (**a**) holo and (**c**) apo *Mt*NifB and schematic presentations of the secondary structural elements of (**b**) holo and (**d**) apo *Mt*NifB. PYMOL was used to prepare the ribbon presentations.[22] The subunits of holo and apo *Mt*NifB are colored light blue and orange, respectively (a, c). The RS-, K1- and K2-clusters are illustrated as ball-and-stick models, with the atoms colored as follows: Fe, orange; S, yellow; O, red; C, grey (a, c). The 2Fo-Fc electron density maps of the representative regions of holo *Mt*MifB and apo *Mt*NifB are shown in Figure S3. The α-helices (labeled H) and β-strands (labeled S) are depicted as yellow tubes and light blue arrows, respectively, and consecutively numbered starting from the N-terminus of the protein; whereas the connecting loops are shown as black lines (b, d). The ligands of the RS-, K1- and K2-clusters are depicted as red, blue and yellow ovals, respectively (b, d). The disordered regions of apo *Mt*NifB are rendered transparent (d). The B-factor putty representation and the B-factor plot of holo *Mt*NifB are shown in Figure S4.

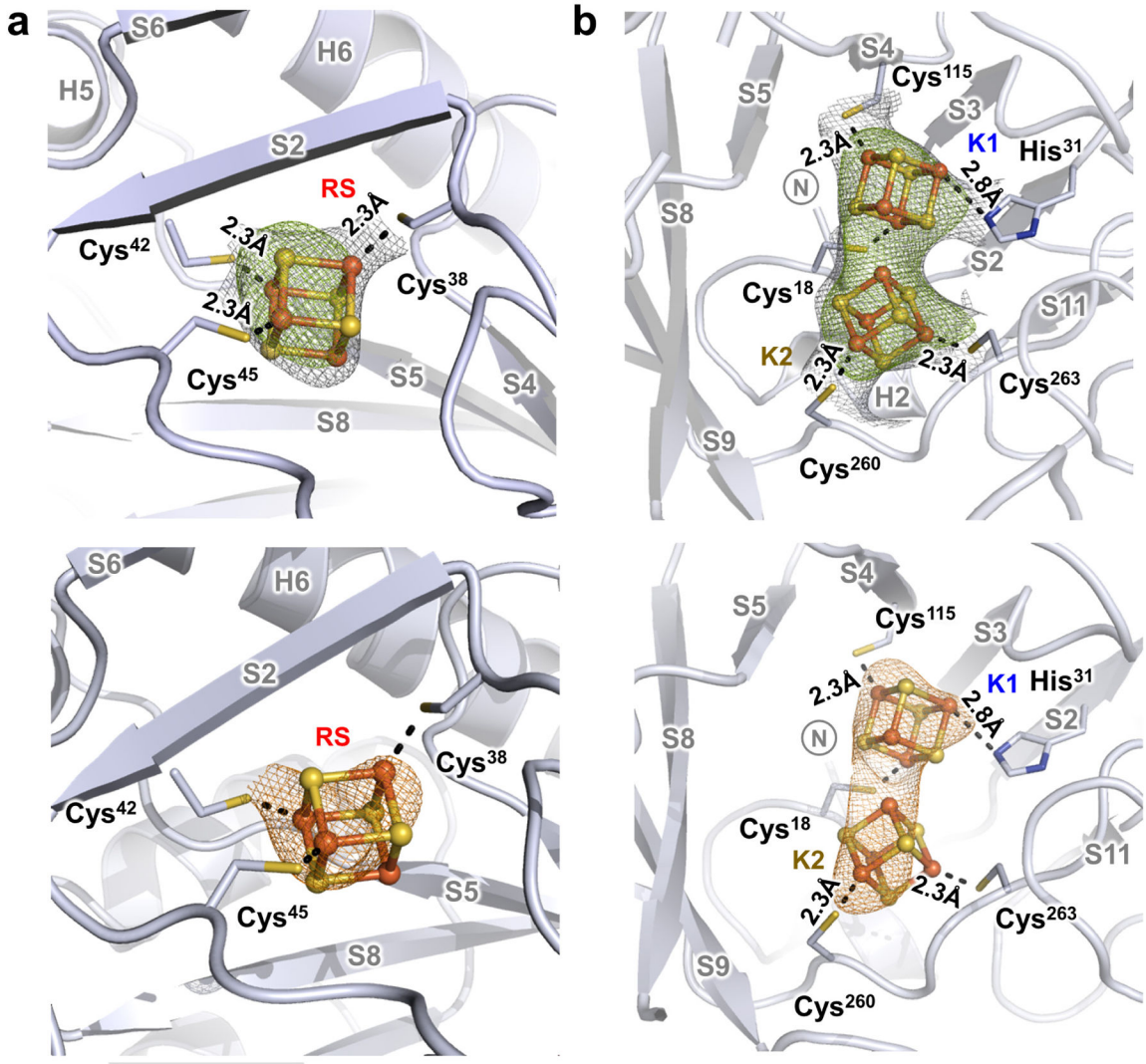

Figure 2.

The three [Fe_4S_4] clusters of holo *Mt*NifB. The structure and ligand coordination of the (**a**) RS- and (**b**) K1- and K2-clusters are depicted and colored as described in Figure 1a. The 2Fo-Fc electron density maps (*upper*, grey mesh, contoured at 1.0 σ), overlaid with the Fo-Fc electron density omit maps (*upper*, green mesh, contoured at 3.0 σ) or the anomalous difference Fourier maps (*lower*, red mesh, contoured at 3.0 σ), clearly indicate the presence of all three [Fe_4S_4] clusters in holo *Mt*NifB (a, b). PYMOL was used to generate this figure. [22] See Table S2 for cluster occupancy.

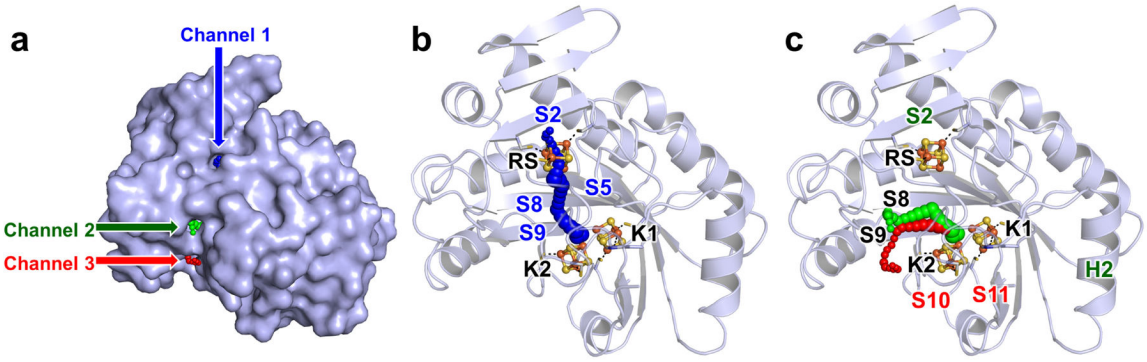

Figure 3.

Predicted substrate channels in holo *Mt*NifB. (**a**) Surface and (**b**, **c**) ribbon presentations of holo *Mt*NifB with the top three channels predicted by CAVER 3.0.3[23] shown as strings of blue (Channel 1), green (Channel 2) and red (Channel 3) spheres, respectively, and the entrances to these channels indicated by arrows of corresponding colors. All three channels extend from the protein surface to K2, with Channel 1 being mostly perpendicular to β-strands S2, S5, S8 and S9 (b), and Channels 2 and 3 being mostly parallel to β-strands S8 and S9 (c). Note the close location of the entrance of Channel 1 to the RS-cluster (b). PYMOL was used to generate this figure.[22] The peptides and clusters of holo *Mt*NifB are depicted and colored as described in Figure 1a.

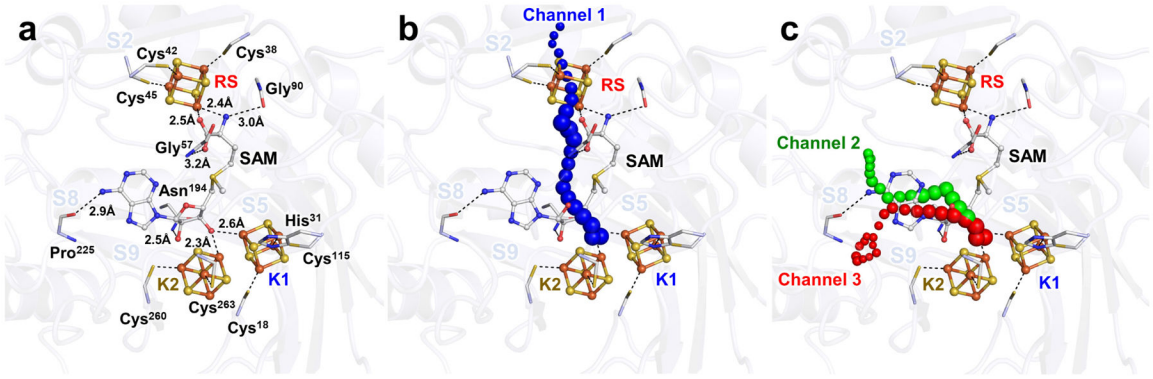

Figure 4.

Model of holo *Mt*NifB bound with SAM. (**a**) Close-up of the modeled SAM-binding site between the RS-cluster and the K1/K2-modules and (**b**, **c**) overlay of Channel 1 (b) and Channels 2 and 3 (c) with the SAM-binding region. PYMOL was used to generate this figure.[22] Binding of SAM was modeled using GLIDE[24] in Maestro 12.4.[25] Based on our model, SAM interacts with the following conserved residues in holo *Mt*NifB that are part of the structural motifs that bind SAM in other known radical SAM (rSAM) enzymes[8]: (*i*) Gly^{90}, part of a 'GDA sequence' that corresponds to the 'GGE motif' of the 'β-strand 2 region' that anchors the amino group of SAM in other rSAM enzymes; (*ii*) Asn^{194}, the location of which corresponds to the 'β-strand 5 region' that interacts with one ribose hydroxyl group of SAM in other rSAM enzymes; and (*iii*) Pro^{225}, the location of which corresponds to 'the β-strand 6 region' that ligates adenine moiety in other rSAM enzymes. Additionally, SAM is further stabilized through unique interactions with other residues/elements in holo *Mt*NifB: (*i*) Gly^{57}, which interacts with the carboxylate group of SAM in a location corresponding to the 'β-strand 1 region' in other rSAM enzymes; and (*ii*) two Fe atoms, one each from the K1- and K2-clusters, which interact with one ribose hydroxyl group in a location previously unseen in other rSAM enzymes. Ligation of SAM by these cluster Fe atoms could result from an 'inward' folding of the N- and C-termini into the barrel region of holo *Mt*NifB, which allows these termini to participate in the binding of the K1- and K2-clusters, positioning them in place for the subsequent interaction with SAM. Such an 'inward' folding of the two termini of the protein has not been observed in other rSAM enzymes, which may be uniquely required for the reaction between SAM and the substrate K1/K2 clusters during the process of carbide insertion in holo *Mt*NifB. The clusters and SAM are shown in ball-and-stick presentations, and the coordinating ligands are shown as sticks. The atoms are colored as described in Figure 1a, and the channels are depicted as described in Figure 3. The peptides are shown in ribbon presentation and rendered transparent in the background.